

High Affinity Radiopharmaceuticals Based Upon Lansoprazole for PET Imaging of Aggregated Tau in Alzheimer's Disease and Progressive Supranuclear Palsy: Synthesis, Preclinical Evaluation, and Lead Selection

Maria V. Fawaz,[†] Allen F. Brooks,^{†,||} Melissa E. Rodnick,^{†,||} Garrett M. Carpenter,[†] Xia Shao,[†] Timothy J. Desmond,[†] Phillip Sherman,[†] Carole A. Quesada,[†] Brian G. Hockley,[†] Michael R. Kilbourn,[†] Roger L. Albin,^{‡,§,¶} Kirk A. Frey,[†] and Peter J. H. Scott*,^{†,¶}

[†]Division of Nuclear Medicine, Department of Radiology, University of Michigan Medical School, Ann Arbor, Michigan 48109, United States

[‡]Geriatrics Research, Education and Clinical Center, Veterans Affairs Ann Arbor Healthcare System, Ann Arbor, Michigan 48105, United States

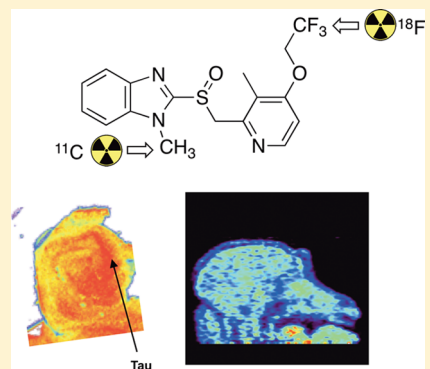
[§]Department of Neurology, The University of Michigan Medical School, Ann Arbor, Michigan 48109, United States

[¶]Michigan Alzheimer Disease Center and [¶]The Interdepartmental Program in Medicinal Chemistry, The University of Michigan, Ann Arbor, Michigan 48109, United States

Supporting Information

ABSTRACT: Abnormally aggregated tau is the hallmark pathology of tauopathy neurodegenerative disorders and is a target for development of both diagnostic tools and therapeutic strategies across the tauopathy disease spectrum. Development of carbon-11- or fluorine-18-labeled radiotracers with appropriate affinity and specificity for tau would allow noninvasive quantification of tau burden using positron emission tomography (PET) imaging. We have synthesized [¹⁸F]lansoprazole, [¹¹C]N-methyl lansoprazole, and [¹⁸F]N-methyl lansoprazole and identified them as high affinity radiotracers for tau with low to subnanomolar binding affinities. Herein, we report radiosyntheses and extensive preclinical evaluation with the aim of selecting a lead radiotracer for translation into human PET imaging trials. We demonstrate that [¹⁸F] N-methyl lansoprazole, on account of the favorable half-life of fluorine-18 and its rapid brain entry in nonhuman primates, favorable kinetics, low white matter binding, and selectivity for binding to tau over amyloid, is the lead compound for progression into clinical trials.

KEYWORDS: Alzheimer's disease, tauopathies, neuroimaging, positron emission tomography imaging, carbon-11, fluorine-18



Statistics from the World Health Organization suggest that in 2012, approximately 36 million people worldwide suffer from some form of dementia. Dementia prevalence is predicted to rise to 115 million by 2050. The most common form is Alzheimer's disease (AD), accounting for ~60% of the dementia landscape, of which there are currently over ~3.8 million cases in the United States alone.¹ Development of therapeutic strategies for neurodegenerative disorders comprising the majority of dementias has proven difficult, partly because the complex interrelated biochemical pathways underlying such disorders are not entirely understood and partly because these disorders manifest clinically overlapping features. Current clinical diagnostic accuracy is 60–80%, indicating that patients often receive an incorrect clinical diagnosis and, historically, definitive diagnosis has only been achieved postmortem.² This issue has a significant impact on therapy development for dementias because wrong diagnosis leads to inappropriate subjects enrolled in clinical trials and negatively

impacts trial outcomes. Bapineuzumab (an antibody targeted against the N-terminus of amyloid β) is a passive immunotherapy that was being tested as a therapeutic for Alzheimer's disease. In a recent clinical trial of bapineuzumab, 15% of patients selected by expert clinicians were later found to be amyloid negative.³

In response to the challenge of improving the accuracy of diagnoses in dementia, significant work has been undertaken to develop radiopharmaceuticals that would allow noninvasive imaging of dementias such as AD using positron emission tomography (PET) imaging. The goals of applying PET in this context are (a) accurate diagnosis of the neurodegenerative disorder while subjects are still alive and, ideally, before the

Received: May 10, 2014

Revised: June 4, 2014

Published: June 4, 2014

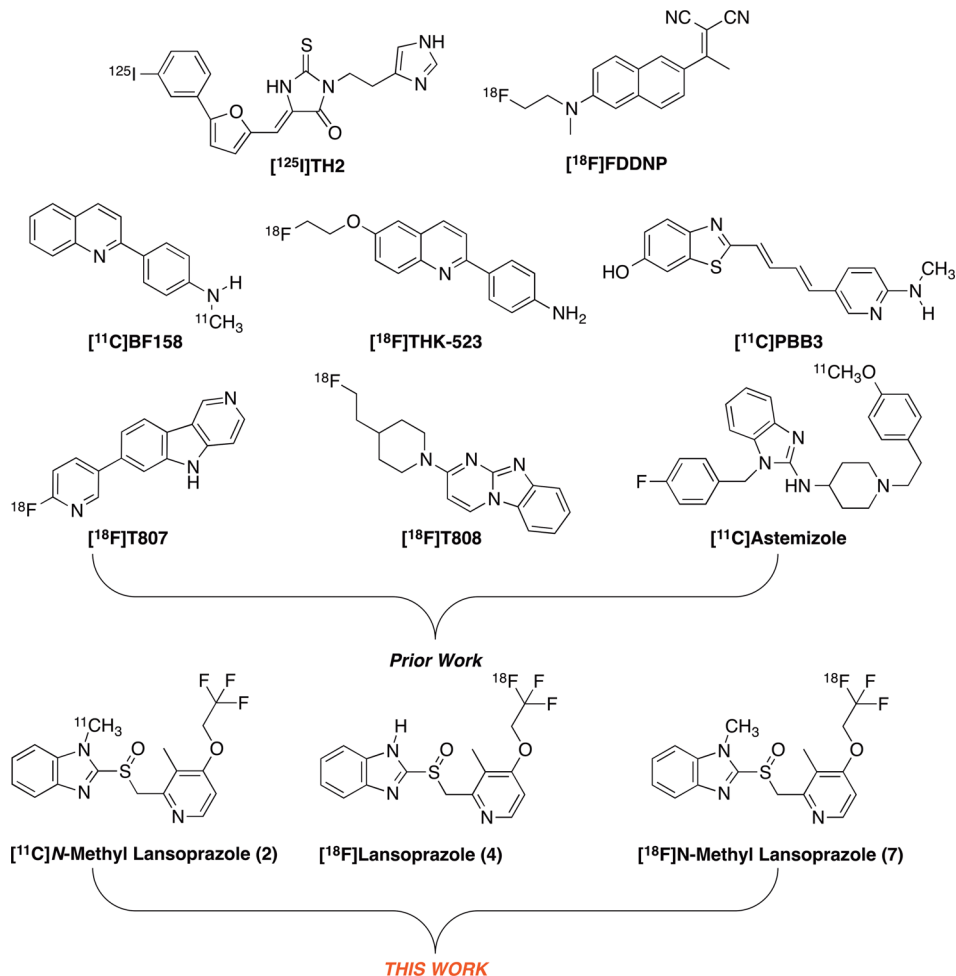


Figure 1. Radiotracers for imaging tau.

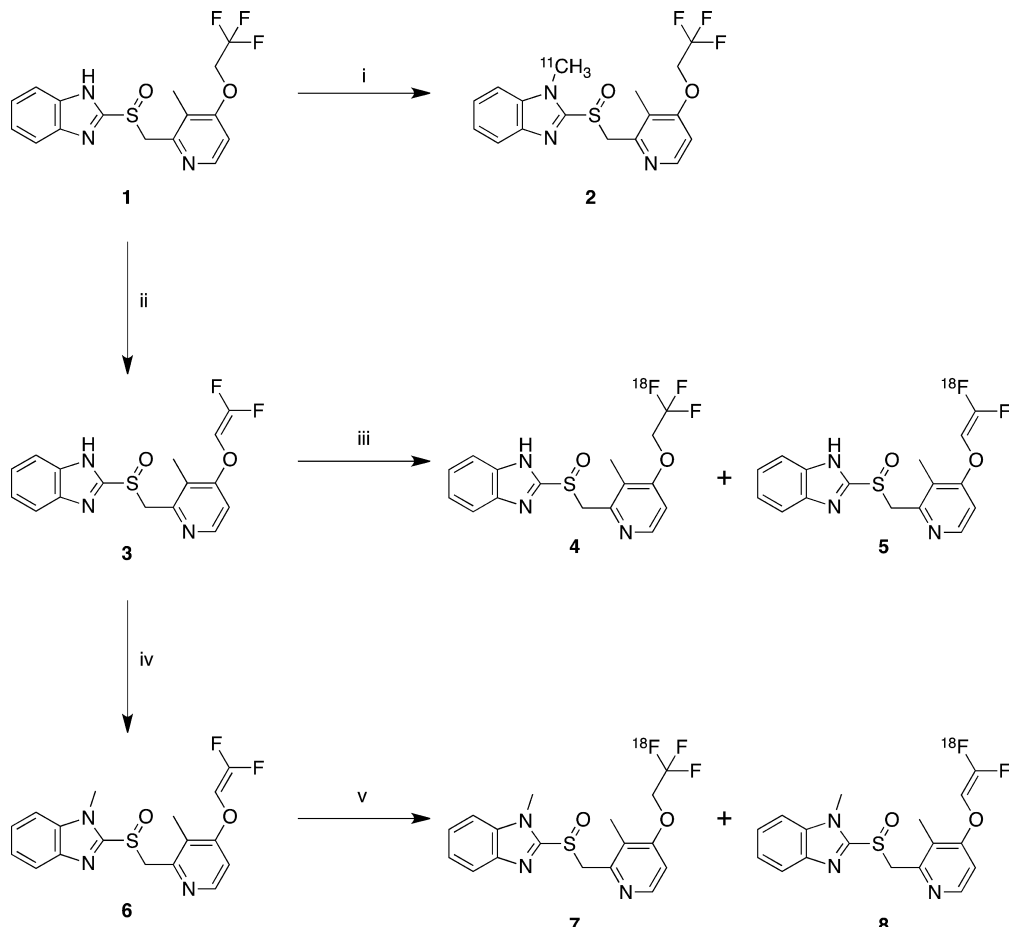
onset of cognitive decline when initiation of a treatment will likely have the best outcome, (b) selection of appropriate subjects for clinical trials, and (c) monitoring subject response to interventions.

In the context of dementias, most efforts are focused upon developing radiopharmaceuticals that target amyloid plaques. $[^{11}\text{C}]$ Pittsburgh Compound B ($[^{11}\text{C}]$ PIB) was the prototypical PET radiotracer for amyloid.⁴ Based upon thioflavin, a pathological dye for amyloid, $[^{11}\text{C}]$ PIB has been used to confirm presence or absence of amyloid in thousands of patients to date. This spearheaded commercial development of a number of amyloid radiotracers, including AMYViD (Florbetapir F18 Injection, Eli Lilly/Avid Radiopharmaceuticals),⁵ Vizamyl (Flutemetamol F18 Injection, GE Healthcare),⁶ and Neuraceq (Florbetaben F18 Injection, Piramal Imaging),⁷ which are all FDA approved. These agents enable noninvasive confirmation of the presence or absence of amyloid plaques (a hallmark pathology of AD) and allow subject stratification based on knowledge of cerebral amyloid burden.³

As more than one neurodegenerative disorder is associated with amyloid pathology [e.g., AD and dementia with Lewy bodies (DLB)], amyloid imaging alone is not sufficient to differentiate dementia subtypes. It is known, moreover, that amyloid plaque burden does not correlate with cognitive status in AD.⁸ Several groups demonstrated that tau neurofibrillary tangle (NFT) burden does correlate with cognitive decline in AD, confirming tau NFTs as a viable target for therapy and

diagnostic PET imaging. Aggregated tau is implicated also in several other dementias, including some forms of frontotemporal dementia (FTD), as well as in neurodegenerative movement disorders such as progressive supranuclear palsy (PSP) and corticobasal degeneration (CBD).⁹ A radiopharmaceutical quantifying aggregated tau burden would aid in the understanding of the pathophysiology and clinical management of each of these neurodegenerations. Beyond improving diagnosis, a successful aggregated tau radiotracer might be useful as a biomarker of disease activity and target engagement.

A critical next phase in PET imaging of dementias is development of radiotracers for estimating tau burden. Despite this, development of radiopharmaceuticals for tau NFTs has been limited and candidate radiopharmaceuticals are currently in the preclinical or early clinical trial stages (Figure 1). Radiotracers for single photon emission computed tomography (SPECT) imaging of tau, such as $[^{125}\text{I}]$ TH2, have been reported¹⁰ but, reflecting the higher sensitivity of PET imaging, most efforts to date have focused on developing PET radiotracers. Okamura and colleagues screened >2000 compounds against tau and identified quinolines and benzimidazoles as scaffolds of interest.¹¹ A number of groups are developing the quinoline scaffold, and both $[^{11}\text{C}]$ BF158¹¹ and the $[^{18}\text{F}]$ THK series, of which a number are under early clinical evaluation,^{12–14} have affinity for tau and selectivity for tau over amyloid. Other scaffolds have been explored. $[^{18}\text{F}]$ T807^{15,16}

Scheme 1. Synthesis of [¹¹C]N-Methyl Lansoprazole and [¹⁸F]Lansoprazole^a

^aReagents and conditions: (i) ^{[11}C]MeOTf, THF, 5 min, rt [loop chemistry], semipreparative HPLC, SPE, 4.6% radiochemical yield. (ii) *n*-BuLi (3 equiv), THF-hexanes, -78 °C, 45 min, 22%. (iii) ^[18]F-fluoride, K₂CO₃, K-2.2.2, solvent, additive (see Table 1), 3–10 min, 90 °C, semipreparative HPLC, SPE, 0.5–14% combined radiochemical yield. (iv) MeI, DBU, CH₂Cl₂, 50%. (v) ^[18]F-fluoride, K₂CO₃, K-2.2.2, solvent, additive (see Table 1), 3–10 min, 90 °C, semipreparative HPLC, SPE, 1–28% combined radiochemical yield.

and [¹⁸F]T808^{17,18} were reported by Kolb et al. and early clinical imaging data in AD subjects suggested radiotracer accumulation in brain areas confirmed to contain tau during postmortem analysis. [¹¹C]PBB3 was reported by Higuchi and colleagues and suggested to bind tau in AD and CBD patients in a first-in-man study.¹⁹ Finally, [¹⁸F]FDDNP is an older radiopharmaceutical found to have affinity for both tau tangles and amyloid plaques.²⁰ As these two protein aggregates can be codistributed in AD, this has limited the utility of this radiotracer to date, although a recent report suggests that [¹⁸F]FDDNP has potential utility in imaging of pure tauopathies.²¹

A recent report from Rojo and co-workers indicated that lansoprazole and astemizole have nanomolar affinity for certain forms of tau and selectivity for tau over amyloid.²² Both compounds contain a benzimidazole moiety, in agreement with the findings of Okamura et al., that the benzimidazole heterocycle is a scaffold of interest for developing compounds with affinity for tau. Riss and co-workers developed radiopharmaceuticals based upon the astemizole scaffold,²³ whereas our group has explored the possibility of repurposing lansoprazole, an FDA-approved proton-pump inhibitor, for PET imaging of aggregated tau. In a preliminary communication, we reported synthesis and initial evaluation of [¹¹C]N-

methyl lansoprazole (2, [¹¹C]NML), demonstrating that it has very high affinity ($K_d = 0.7$ nM) for heparin-induced tau filaments (HITF).²⁴ For a PET radiotracer to receive widespread adoption, however, it should be radiolabeled with fluorine-18 (half-life = 109.77 min) rather than carbon-11 (half-life = 20.38 min), as the longer half-life enables regional distribution of the radiopharmaceutical to imaging facilities without a cyclotron. Additionally, a tau radiotracer should cross the blood-brain barrier, have selectivity for tau when compared to amyloid since aggregated versions of both proteins coexist in Alzheimer's disease, and have minimal nonspecific white matter binding.^{25–27} This paper builds on our initial communication, reporting the synthesis of [¹⁸F]lansoprazole (4, [¹⁸F]LNS) and [¹⁸F]N-methyl lansoprazole (7, [¹⁸F]NML). Extensive preclinical evaluation of all three radiotracers in the series has also been undertaken with the goal of identifying the lead compound for translation into human imaging trials.

RESULTS AND DISCUSSION

Chemistry. When considering how to radiolabel lansoprazole (1), it was apparent that the molecule could either be labeled with carbon-11 by methylation of the benzimidazole moiety, or with fluorine-18 by incorporation into the trifluoromethyl group. The former was readily achieved by

Table 1. Conditions for the Radiosynthesis of [¹⁸F]Lansoprazole

entry	precursor	reaction conditions	combined RCY of CF ₃ and =CF ₂ ^a	ratio of CF ₃ to =CF ₂
1	3	1 mL DMSO; 90 °C; 3 min	1–3% (<i>n</i> = 4)	1:10
2	3	950 μL DMSO: 50 μL H ₂ O; 90 °C; 3 min	0.5% (<i>n</i> = 1)	1:1
3	3	950 μL DMSO + 10 μL IPA; 90 °C; 3 min	4–7.5% (<i>n</i> = 6)	1:10
4	3	950 μL DMSO + 15 μL IPA; 90 °C; 3 min	6% (<i>n</i> = 1)	1:10
5	3	500 μL DMSO + 36 μL IPA; 90 °C; 10 min	4–14% (<i>n</i> = 3)	1:1
6	3	1 mL THF; 90 °C, 3 min	0% (<i>n</i> = 1)	N/A
7	3	1 mL MeCN; 90 °C, 3 min	0% (<i>n</i> = 1)	N/A
8	3	950 μL DMSO + 5 μL satd. NH ₄ Cl; 90 °C, 3 min	8–12% (<i>n</i> = 3)	1:4
9	6	1 mL DMSO; 90 °C; 3 min	1–6% (<i>n</i> = 4)	1:10–1:100
10	6	500 μL DMSO + 36 μL IPA; 90 °C; 10 min	0% (<i>n</i> = 4)	N/A
11	6	950 μL DMSO + 5 μL satd. NH ₄ Cl; 90 °C, 3 min	12–28% (<i>n</i> = 4)	1:3
12	6	950 μL DMSO + 5 μL 7 M NH ₄ OTf; 90 °C, 3 min	9% (<i>n</i> = 1)	1:6

^aNondecay-corrected radiochemical yield at end-of-synthesis based upon 900 mCi of [¹⁸F]fluoride

methylation with [¹¹C]MeOTf (Scheme 1), and [¹¹C]N-methyl lansoprazole (2) was obtained in 4.6% non-decay-corrected radiochemical yield (RCY), based upon [¹¹C]methyl iodide, with 99% radiochemical purity and specific activities >15 000 Ci/mmol, as reported in our preliminary communication (*n* = 5).²⁴ We were also interested in synthesizing fluorine-18 labeled derivatives for the reasons outlined above.

The synthesis of [¹⁸F]lansoprazole was reported in a 2010 patent using an isotopic exchange with lansoprazole.²⁸ However, no further work with [¹⁸F]lansoprazole has been reported since that patent disclosure. Isotopic exchange is not an ideal method for preparing fluorine-18 radiolabeled compounds because of the large amounts of cold mass that are unavoidable in the final product, leading to poor specific activities. Therefore, development of a synthesis of [¹⁸F]-lansoprazole in our laboratory concentrated on adaptation of recent chemistry reported by Riss and co-workers.^{29,30} They were able to generate [¹⁸F]trifluoroalkyl tosylates labeled at the trifluoromethyl group by reacting the corresponding gem-difluoroalkene with [¹⁸F]fluoride, potassium carbonate and Kryptofix 2.2.2. The [¹⁸F]trifluoroalkyl tosylates were utilized as prosthetic groups for radiolabeling larger molecules. Although this approach could hypothetically be used to synthesize [¹⁸F]lansoprazole, it would require a lengthy synthesis of the corresponding pyridinolic precursor. We focused on conversion of commercially available lansoprazole (1) to the gem-difluoroalkene derivative of lansoprazole (3) as an operationally simpler approach to [¹⁸F]lansoprazole (4). Initially, lansoprazole was subjected to 2 equiv of *n*-BuLi, per the literature procedure. However, starting material was recovered initially, and longer reaction times resulted in decomposition by-products. The poor reaction was attributed to unwanted consumption of *n*-BuLi resulting from deprotonation of the benzimidazole. Increasing the quantity of *n*-BuLi to 3 equiv provided gem-difluoroalkene (3) in 22% yield without the need for any protecting groups (Scheme 1).

The gem-difluoroalkene precursor was reacted with [¹⁸F]-fluoride in the presence of potassium carbonate and Kryptofix 2.2.2, in anhydrous dimethyl sulfoxide (DMSO) (Scheme 1). Under these conditions, [¹⁸F]lansoprazole (4) and [¹⁸F]gem-difluoroalkene (5) were obtained in 1–3% combined radiochemical yield (Table 1, Entry 1). The ratio of 4:5 was 1:10, consistent with the findings of Riss and suggesting that the anhydrous conditions favored generation of the radiolabeled alkene via an addition–elimination mechanism similar to that proposed by Pike and co-workers in their early work with

related chemistry.³¹ To overcome this problem, Riss noted that protic additives favored synthesis of the trifluoromethyl derivatives over the alkene, presumably by quenching the intermediate anion before it could eliminate a fluoride. This also proved to be the case in our hands (Table 1), and repeating the fluorination reaction in 95% DMSO:5% water resulted in 4 and 5 in a 1:1 ratio (Table 1, Entry 2). However, the high water concentration was detrimental to the reaction yield. More promising results were obtained when DMSO containing isopropanol (IPA) was used as the reaction solvent. Adding 1–1.5% of isopropanol to the DMSO resulted in higher combined yields of 4 and 5 (Table 1, Entries 3 and 4), but in both cases, the ratio was still 10:1 in favor of the alkene side product. The effects of concentration and reaction time were also investigated. The optimal reaction conditions were established as 5% isopropanol in 0.5 mL of DMSO at 90 °C for 10 min (Table 1, Entry 5), providing 4 and 5 in a 1:1 ratio and up to 14% combined radiochemical yield. Interestingly, unlike Riss, we have been unable to drive the product ratio above 1:1 in favor of the trifluoromethyl species 4, and we attribute this to the different substrates being radiolabeled. The intermediate carbanion in the synthesis of [¹⁸F]lansoprazole is adjacent to three fluorine atoms and lone pairs of electrons of the oxygen atom. The carbanion is expected to be short-lived and intramolecular elimination appears favored over intermolecular proton capture. Contrastingly, the lone pairs on the adjacent oxygen atom in Riss's substrate can be expected to have some resonance delocalization into the sulfonate group.²⁹ This resonance presumably imparts sufficient stability to the intermediate carbanion so as to favor generation of the trifluoromethylated product. Unlike Riss's reported reactions, the synthesis of [¹⁸F]lansoprazole did not proceed in tetrahydrofuran (Entry 6) or acetonitrile (Entry 7).

With an established synthesis available, attention was turned to identifying a suitable HPLC method for purification of [¹⁸F]lansoprazole, which was expected to be somewhat challenging given the structural similarities of 4 and 5. Not surprisingly, traditional reverse-HPLC stationary phases proved unsuitable for the purification, and the separation of 4 and 5 was not achievable. As a key difference between the two products was the fluorine content, a perfluorophenyl-capped matrix was next investigated as the stationary phase (Luna-PFP(2), Phenomenex). This was found to be the method of choice, and baseline separation between 4 and 5 was obtained in both the semipreparative and analytical cases (see representative HPLC traces in the Supporting Information).

Final reformulation of the collected HPLC fraction using a C18 Sep-Pak provided [¹⁸F]lansoprazole in 2–7% (nondecay-corrected radiochemical yield at end-of-synthesis, based upon 900 mCi of [¹⁸F]fluoride), with >95% radiochemical purity and specific activities reaching a maximum of 1000 Ci/mmol.

We next concentrated on the synthesis of [¹⁸F]*N*-methyl lansoprazole (**7**). The requisite precursor **6** was accessed by simple methylation of compound **3**, which proceeded in 50% yield. Separate attempts to generate **6** by treatment of *N*-methyl lansoprazole with BuLi were unsuccessful, leading only to complex mixtures of decomposition byproducts. Subjecting gem-difluoroalkene precursor **6** to fluorination conditions in anhydrous DMSO generated [¹⁸F]*N*-methyl lansoprazole (**7**) and the corresponding [¹⁸F]gem-difluoroalkene (**8**) in 1–6% combined radiochemical yield (Entry 9). The ratio of **7**:**8** was more erratic than [¹⁸F]lansoprazole, ranging from 1:10 to 1:100. We attempted to favor formation of the desired trifluoromethyl product **7** by using the optimal conditions worked out for [¹⁸F]lansoprazole above (5% isopropanol in 0.5 mL of DMSO), but in this case, addition of isopropanol completely inhibited the reaction and neither **7** or **8** were formed (Entry 10). Although further mechanistic studies are required (and ongoing) to understand this result, we considered that excess precursor **3** would have a *pK_a* comparable to lansoprazole (*pK_a* = 8.5) and could act as a proton source in the original reaction described above. Conversely, *N*-methyl lansoprazole does not have a free N–H and cannot act as a proton source. We reasoned that replacing isopropanol (*pK_a* = 17.1) with a protic additive that had a *pK_a* closer to that of lansoprazole would generate [¹⁸F]*N*-methyl lansoprazole. Gratifyingly, this proved to be the case, and repeating the reaction in DMSO (950 μL) spiked with 5 μL of saturated ammonium chloride (*pK_a* = 9.2) generated **7** and **8** in good combined radiochemical yields of 12–28% (Entry 11), and a product ratio of 3:1 in favor of [¹⁸F]gem-difluoroalkene **8**. NH₄OTf could also be used as the proton source (Entry 12), which could be important in the future if chloride-for-fluoride exchange becomes an issue when employing NH₄Cl. The modified reaction conditions were also compatible with the synthesis of [¹⁸F]lansoprazole (Entry 8), but again, we have been unable to favor formation of either trifluoromethylated product over the corresponding gem-difluoroalkene. Purification of [¹⁸F]*N*-methyl lansoprazole was achieved using semipreparative HPLC with the Luna-PFP column and HPLC method described above (see Figure S12 in the Supporting Information for a typical HPLC trace), and final reformulation by C18 Sep-Pak provided [¹⁸F]*N*-methyl lansoprazole in 3–7% (nondecay-corrected radiochemical yield at end-of-synthesis, based upon 900 mCi of [¹⁸F]fluoride), with >95% radiochemical purity and specific activities reaching a maximum of 1000 Ci/mmol (determined at end-of-synthesis).

Specific activities of both fluorinated radiotracers **4** and **7** were up to 50% lower than for typical radiotracers labeled with fluorine-18 in our laboratory. The reasons for this are not clear, but perhaps other nucleophiles (e.g., isopropanol or DMSO) are adding into the alkene precursor and displacing cold fluoride, which is then free to add to additional molecules of the precursor and generate higher amounts of the nonradioactive compound than usual. Nevertheless, specific activities were adequate for preclinical evaluation and further exploration of the reaction mechanism is ongoing and will be reported in due course. All doses were formulated in 5% ethanol and confirmed by additional quality control testing (visual inspection, pH) to

be suitable for preclinical evaluation. Stability testing by repeated HPLC analysis of radiochemical purity also confirmed that [¹⁸F]lansoprazole **4** and [¹⁸F]*N*-methyl lansoprazole **7** were stable for at least 1.5–2 h following end-of-synthesis (see Figures S7 and S14 in Supporting Information).

Biology. Radiotracers with potential for imaging aggregated tau need to have high affinity for tau, but also need to have selectivity for tau when compared to amyloid because aggregated versions of both proteins coexist in Alzheimer's disease. The affinities of the three candidate radiotracers for both heparin-induced tau filaments and aggregated A β_{1-42} were evaluated by determining *K_d* (Table 2), and for both proteins,

Table 2. Binding Affinity Data^a

	<i>K_d</i> (HITF) ^b	<i>B_{max}/K_d</i> (tau) ^c	<i>K_d</i> (Aggregated A β_{1-42}) ^d	<i>B_{max}/K_d</i> (amyloid) ^e	<i>K_d</i> amyloid/ <i>K_d</i> tau
[¹¹ C]NML/ [¹⁸ F]NML	0.7 nM	71	8.2 nM	49	11.7
[¹⁸ F]LNS	3.3 nM	15	11.0 nM	36	3.3

^aMean data from two experiments. ^bHuman Tau 441. ^cAssuming 50 nM of tau. ^dMouse A β_{1-42} . ^eAssuming 400 nM of amyloid.

the data was consistent with one-site binding. Each compound was found to have very high affinity for heparin-induced tau filaments (low to subnanomolar), with the *N*-methyl lansoprazole derivatives having a 4.7-fold higher affinity than lansoprazole. The *K_d* of *N*-methyl lansoprazole for heparin-induced tau filaments was 0.7 nM, which makes them the highest affinity radiotracers for tau reported to date. Lansoprazole had slightly lower affinity for heparin-induced tau filaments (*K_d* = 3.3 nM, consistent with a *K_i* of 2.3 nM reported by Rojo et al.²²).

As tau aggregates are often codistributed with amyloid plaques in Alzheimer's disease, a tau-imaging agent should also be selective for tau over amyloid. Conducting analogous binding affinity experiments with aggregated A β_{1-42} revealed lower affinities for that protein. The *K_d* of the *N*-methyl lansoprazole derivatives for amyloid was 8.2 nM, whereas the *K_d* for and [¹⁸F]lansoprazole for was 11.0 nM. Thus, using *K_d*(amyloid)/*K_d*(tau) as an estimate of selectivity for tau over amyloid suggests 11.7-fold selectivity for [¹¹C]*N*-methyl lansoprazole and [¹⁸F]*N*-methyl lansoprazole and 3.3-fold selectivity for [¹⁸F]lansoprazole.

The binding potential (BP), estimated by the *B_{max}/K_d* value, is a useful criterion when considering the suitability of a radiotracer for imaging a target binding site in human subjects. Although the ideal binding potential is unknown, useful radiotracers have a binding potential that falls within a range of values,³² although ≥ 5 has recently been recommended for CNS radiotracers by the National Institutes of Health. We have adopted this latter value for the purposes of evaluating the new radiotracers described herein. The amount of aggregated tau (as paired helical filaments) in AD brain is reported to be between 50 and 200 nmol/kg in wet tissue (taking the lower end, *B_{max}* = 50 nmol/kg wet tissue \sim 50 nmol/L or 50 nM),^{25,33} so a tau radiotracer should have a *K_d* \leq 10 nM for *B_{max}/K_d* \geq 5, and that would require the radiotracer to have very low nonspecific binding to succeed as a PET radiotracer. We have previously reported that the *B_{max}* of [¹¹C]*N*-methyl lansoprazole for heparin-induced tau filaments was 0.214 fmol/ μ g, which equates to 200 nmol/kg and is consistent with the higher end of estimates of tau in wet tissue.²⁴ Thus, estimated ranges

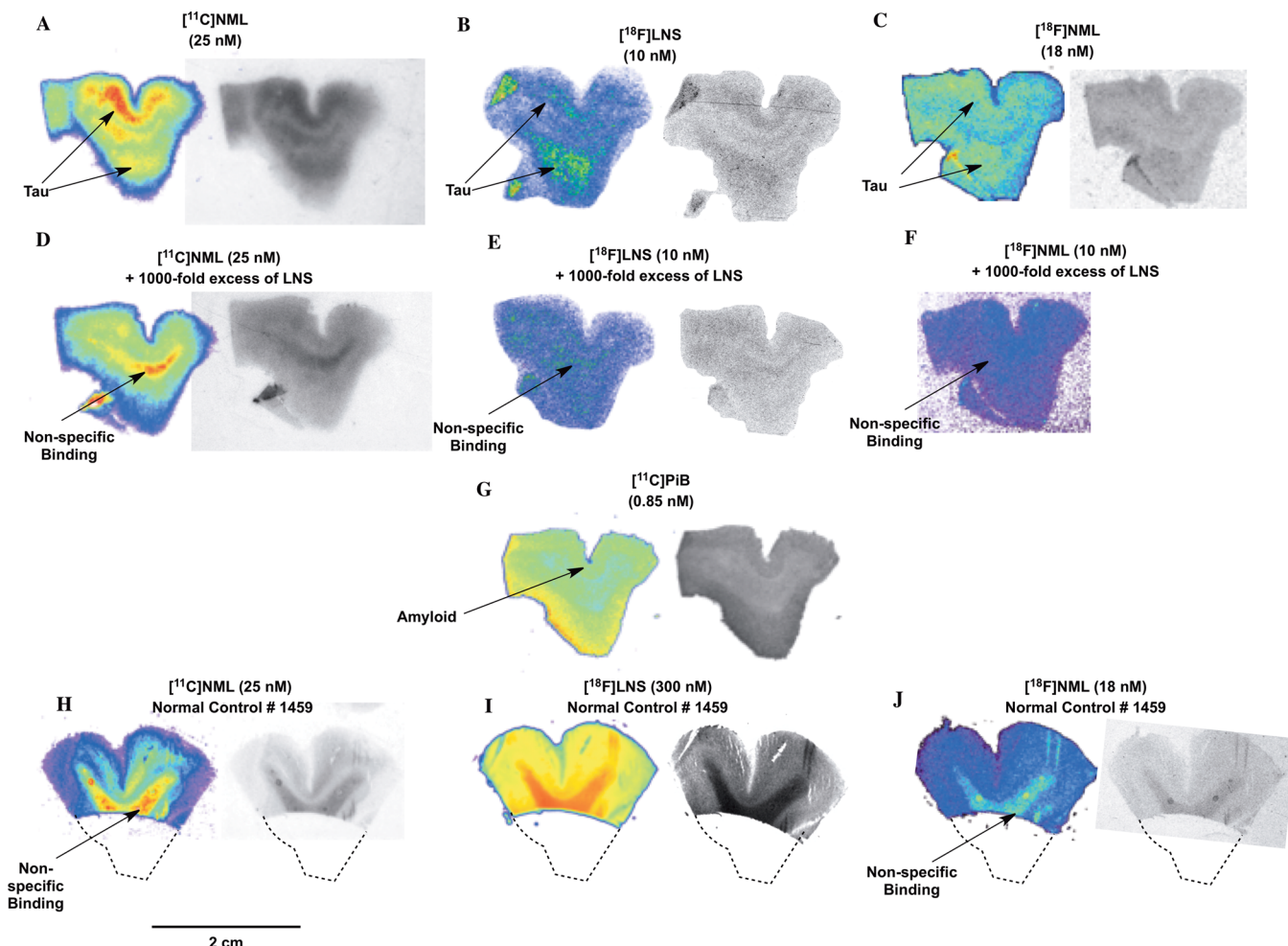


Figure 2. Autoradiographic images of brain samples from AD subject 1649 showing [¹¹C]NML (A), [¹⁸F]LNS (B), and [¹⁸F]NML (C) binding tau NFTs; nonspecific [¹¹C]NML (D), [¹⁸F]LNS (E), and [¹⁸F]NML (F) binding following coincubation with 1000-fold excess of lansoprazole; [¹¹C]PiB (G) binding amyloid plaques; and autoradiographic images of brain samples from normal control 1459 obtained using [¹¹C]NML (H), [¹⁸F]LNS (I) and [¹⁸F]NML (J) (all images were obtained using Kodak BioMax MR film except I, which was an early image obtained using Kodak Amersham film that is less sensitive to β/γ emitters and required a larger amount of radiotracer).

of binding potential against tau for [¹¹C]N-methyl lansoprazole and [¹⁸F]N-methyl lansoprazole is 71–284, whereas the range for [¹⁸F]lansoprazole is 15–60, suggesting suitability of this family of radiotracers for future applications in clinical PET imaging of tau burden.

Determining the B_{\max} for amyloid is a more complicated story. $A\beta_{1-40}$ and $A\beta_{1-42}$ brain concentrations in AD have been estimated at 400–1900 nmol/kg,²⁵ and if the lower number is used it leads to B_{\max}/K_d estimates of 49 and 36 for the *N*-methyl lansoprazole derivatives and [¹⁸F]lansoprazole, respectively (Table 2). However, although $A\beta_{1-40}$ is the more common of the two, $A\beta_{1-42}$ is the more fibrillogenic and, thus, is more commonly associated with senile plaques in AD. Therefore, these binding potential numbers for amyloid may be overestimations in practice, if the concentration of aggregated $A\beta_{1-42}$ plaques are actually $\ll 400$ nmol/kg.

As the in vitro studies had demonstrated that the radiotracers had high affinity for tau and selectivity for tau over amyloid using pure synthetic proteins in vitro, we next wished to determine whether affinity and selectivity translated to the protein forms found in AD by conducting autoradiography on brain tissue samples obtained from the Brain Bank of the Michigan Alzheimer's Disease Center. Tissue samples from

Alzheimer's disease patients were first compared to analogous samples from healthy controls (Figure 2). Inferior frontal cortex sections were selected from two AD patients positive for tau NFTs and amyloid plaques according to their pathology reports (subjects 1650, a 78 year old female and 1649, a 77 year old male), and one healthy control confirmed to be tau and amyloid negative (subject 1459, a 70 year old male). Initially, the tau NFTs and amyloid plaques identified in the pathology reports of the AD patients were confirmed in our laboratory using immunohistochemistry with antitau (H-150) (Santa Cruz Biotechnology Inc.; Figure S15 in Supporting Information) and antibody-amyloid 1-42 (Millipore; Figure S16 in Supporting Information), respectively. Tau NFTs were ubiquitous throughout both AD inferior frontal cortex samples, whereas amyloid plaques were concentrated around the edges of the brain samples. The normal control brain sections were negative for amyloid and tau.

Adjacent sections were then incubated with [¹¹C]N-methyl lansoprazole 2 (Figure 2A), [¹⁸F]lansoprazole 4 (Figure 2B) and [¹⁸F]N-methyl lansoprazole 7 (Figure 2C). The images confirm colocalization of lansoprazole with tau NFTs identified by immunohistochemistry. The images obtained with the carbon-11 radiotracer appear more intense because the specific

activity of that tracer ($>15\,000$ Ci/mmol) is routinely higher than the fluorinated radiotracers (1000 Ci/mmol). Specific and nonspecific binding was investigated by repeating the incubation in the presence of 1000-fold excess of unlabeled lansoprazole. The majority of the signal was due to specific binding of the radiotracers to tau NFTs, but a small amount of nonspecific white matter binding where [^{11}C]N-methyl lansoprazole (Figure 2D), [^{18}F]lansoprazole (Figure 2E), or [^{18}F]N-methyl lansoprazole (Figure 2F) could not be displaced by addition of excess lansoprazole. Nonspecific binding was more apparent at higher concentrations (>25 nM) of radiotracer. To next rule out binding of the radiotracers to amyloid plaques, the plaques were identified by consensus between immunohistochemistry (Figure S16 in Supporting Information) and autoradiography with [^{11}C]Pittsburgh Compound B ([^{11}C]PiB, Figure 2G), an amyloid imaging agent. There was no binding of 2, 4, or 7 to amyloid plaques at the screened concentrations, supporting the selectivity identified in the binding affinity experiments. In the case of the normal control brain samples (Figures 2H, 2I and 2J), no uptake of the radiotracers was seen in gray matter, and only some background autoradiography signals resulting from nonspecific white matter binding were observed.

Significant tau burden is more common in the hippocampus in Alzheimer's disease, and this was apparent in a sample of hippocampus from a third Alzheimer's disease patient (subject 1657, a 87 year old female). This brain sample also contained amyloid plaques, and the presence of both was confirmed by immunohistochemistry. Tau NFTs were fairly uniformly distributed throughout the tissue sample (Figure S17 in Supporting Information), whereas amyloid plaques were concentrated in the subiculum (Figure S18 in Supporting Information). Tissues samples were incubated with both [^{18}F]lansoprazole and [^{11}C]Pittsburgh Compound B (Figure 3). In studies with [^{11}C]PiB, amyloid plaques were detected

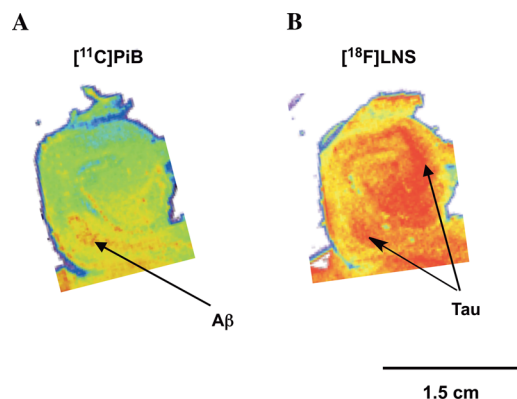


Figure 3. Autoradiographic images of brain samples from AD subject 1657 showing [^{11}C]PiB binding to amyloid plaques (A); and [^{18}F]LNS binding to tau NFTs (B).

only in the subiculum (Figure 3A), whereas [^{18}F]lansoprazole identified tau NFTs prevalent throughout the entire hippocampus (Figure 3B). This is in agreement with the significant hippocampal uptake of [^{11}C]PBB3 reported in initial clinical findings by Higuchi and co-workers.¹⁹ The colocalization of [^{11}C]PiB and [^{18}F]lansoprazole in the subiculum of the hippocampus results from the coexistence of tau NFTs and amyloid plaques at the interface between the hippocampus and

the cortex, confirmed by immunohistochemistry (Figures S17 and S18 in Supporting Information). To summarize AD autoradiography, adjacent brain sections were double immunostained for tau and amyloid, and were compared with [^{11}C]NML, [^{18}F]NML, and [^{18}F]LNS autoradiography. In all AD tissue sections examined, positive lansoprazole signals colocalized with tau immunostaining but not with amyloid plaques, as indicated.

Beyond Alzheimer's disease, aggregated tau pathology is implicated in a range of neurodegenerative disorders known collectively as tauopathies, but the tau isoforms present in each disorder are different. We have previously demonstrated that [^{11}C]N-methyl lansoprazole binds to tau in brain samples from progressive supranuclear palsy (PSP) patients,²⁴ and wanted to also confirm that this was the case for [^{18}F]lansoprazole. In PSP, tau aggregates as globose tangles and/or tufted astrocytes, and the globus pallidus brain samples utilized in this work (subject 6867, a 71 year old female) was found to have both forms of tau throughout the whole section, confirmed by immunohistochemistry. This was reflected in uniform uptake of [^{18}F]lansoprazole (Figure 4A), the majority of which was

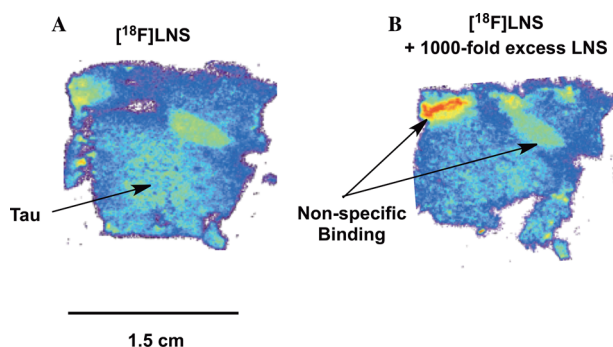


Figure 4. Autoradiographical images of brain samples from PSP subject 6867 showing [^{18}F]LNS binding tau globose tangles and tufted astrocytes (A); and nonspecific [^{18}F]LNS following coinubcation with 1000-fold excess of lansoprazole (B).

specific binding, although like the AD brains there was evidence of some nonspecific white matter binding that could not be displaced by incubation with 1000-fold excess concentration of lansoprazole (Figure 4B).

The strong agreement between the autoradiography data obtained using tau-positive human brain samples from both AD and PSP patients, and in vitro binding data obtained using heparin-induced tau filaments was particularly gratifying in these studies. In addition to validating lansoprazole as a scaffold for developing tau radiotracers, this agreement also suggests that heparin-induced tau could be a straightforward and economical tool for screening compound libraries for affinity against tau.

In vivo behavior of the radiotracers were investigated in rodents and nonhuman primates, including imaging properties, biodistribution, and metabolism. We reported previously that N-methyl lansoprazole is metabolized slowly and that we detected a single polar metabolite that is likely the hydroxy or sulfone derivative, consistent with the known metabolism of lansoprazole. Additionally, N-methyl lansoprazole is excreted via both the liver and the kidneys, in agreement with the established excretion of lansoprazole.^{24,34–39} [^{11}C]N-Methyl lansoprazole is a substrate for the rodent permeability-glycoprotein 1 (Pgp) transporter (or multidrug resistance

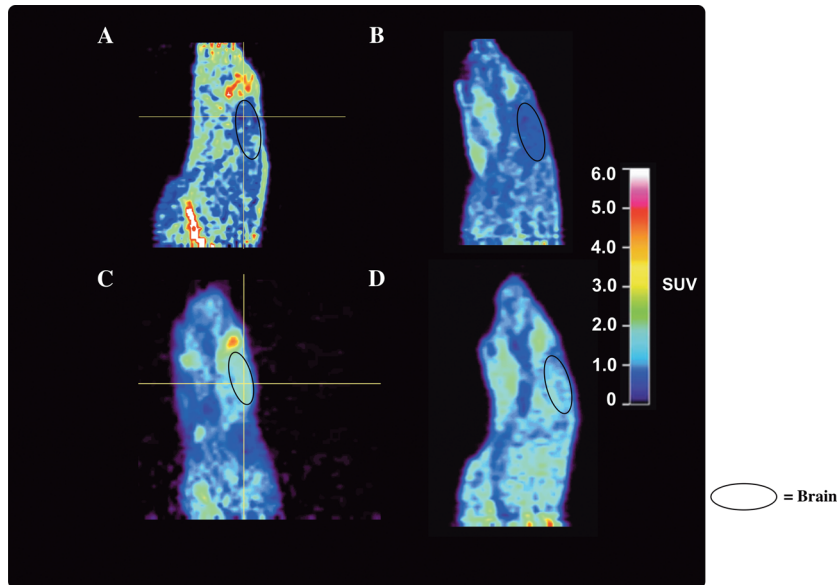


Figure 5. Representative sagittal microPET images of rodents imaged with ^[11C]NML (A, summed images 0–60 min post i.v. injection of the radiotracer), ^[18F]LNS (B, summed images 0–90 min post i.v. injection of the radiotracer), ^[11C]NML following pretreatment with cyclosporin A (C, summed images 0–60 min post i.v. injection of the radiotracer), and ^[18F]LNS following pretreatment with cyclosporin A (D, summed images 0–90 min post i.v. injection of the radiotracer).

protein 1 (MDR1)), which results in no discernible brain uptake of the radiotracer in rats (Figure 5A) despite a known log *P* of 2.18.²⁴ An analogous experiment revealed the same to be true for ^[18F]lansoprazole (Figure 5B), despite a known log *P* of 1.47.²² In the case of both radiotracers, Pgp involvement was confirmed by the increased brain uptake that was apparent when rats were pretreated with 50 mg/kg cyclosporin A, an immunosuppressant known to block Pgp activity (Figure 5C and 5D). Regions-of-interest (ROI) were drawn for the whole brain and used to generate time-radioactivity curves (TACs, Figure 6), which confirmed minimal brain uptake in the

(~0.85 µg/kg) was insufficient to block the Pgp and resulted in no appreciable brain uptake of the radiotracer. Further experiments aimed at understanding the role of efflux transporters in the CNS penetration of these radiotracers are ongoing and will be reported in due course. Whole brain time-radioactivity curves for imaging studies following blockade of the Pgp with cyclosporin A revealed rapid uptake of both ^[11C]N-methyl lansoprazole (peak uptake was ~6879 nCi/cc, corresponding to a peak standardized uptake value (SUV) of 2.25) and ^[18F]lansoprazole (peak uptake was ~2480 nCi/cc, corresponding to a peak SUV of 1.12).

Although ^[11C]N-methyl lansoprazole is a substrate for the rodent Pgp, the radiotracer does enter the rhesus monkey brain (Figure 7A, *n* = 2),²⁴ and analogous imaging results were obtained in nonhuman primates using ^[18F]N-methyl lansoprazole (Figure 7B, *n* = 2). ROI were drawn for the whole brain and used to generate time-radioactivity curves (Figure 8), which revealed rapid uptake of both ^[11C]N-methyl lansoprazole (peak uptake was ~1600 nCi/cc (corresponding to a peak SUV) of 1.69) and ^[18F]N-methyl lansoprazole (peak uptake was ~1500 nCi/cc (corresponding to a peak SUV of 2.02)). Peak uptake occurred within 3 min postinjection, and was followed by virtually complete washout over the duration of the PET scans for each radiotracer. Both radiotracers provided reasonable levels of uptake in all gray matter regions (for example, see Figure 9 for regional time-radioactivity curves of ^[18F]N-methyl lansoprazole), and very little white matter binding was apparent, suggesting that both have potential as CNS radiotracers. The difference in imaging results between rodents and nonhuman primates can be rationalized by recent findings that Pgp transporter expression is significantly higher in rodents than primates.⁴⁰ In both rodent and primates TACs, there are apparent increases in SUV during the last two time points. We see this frequently in our data analysis, independent of radiotracer, and attribute it to increased noise resulting from the low residual counts that remain in the brain during the late frames of the PET scans.

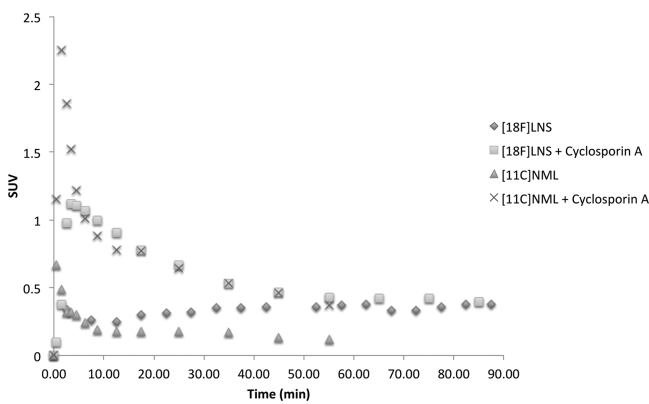


Figure 6. Rodent whole brain time-radioactivity curves for ^[11C]NML and ^[18F]LNS with and without cyclosporin A pretreatment.

baseline scans for either radiotracer. The lack of brain uptake is consistent with quantitative *in vivo* biodistribution data that we have previously reported for *N*-methyl lansoprazole,²⁴ but contrasts the brain uptake of lansoprazole reported by Rojo and co-workers.²² It is possible that the dose of lansoprazole used in the latter pharmacokinetic experiments (16 mg/kg) was sufficient to saturate the Pgp and promote brain uptake, whereas the microdose administered during the PET scans

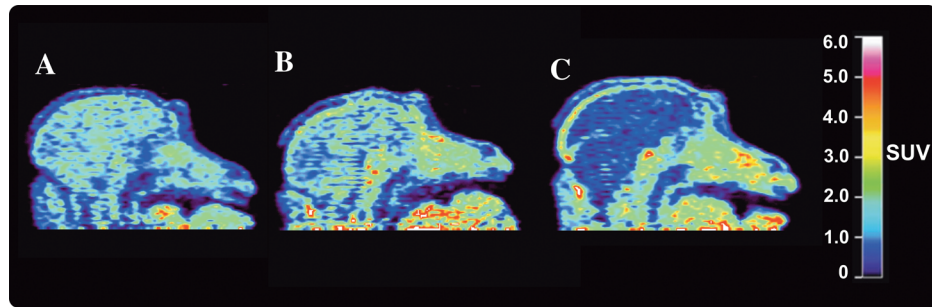


Figure 7. Representative sagittal microPET images of nonhuman primates imaged with $[^{11}\text{C}]$ NML (A, summed images 0–60 min post i.v. injection of the radiotracer), $[^{18}\text{F}]$ NML (B, summed images 0–90 min post i.v. injection of the radiotracer) and $[^{18}\text{F}]$ LNS (C, summed images 0–60 min post i.v. injection of the radiotracer).

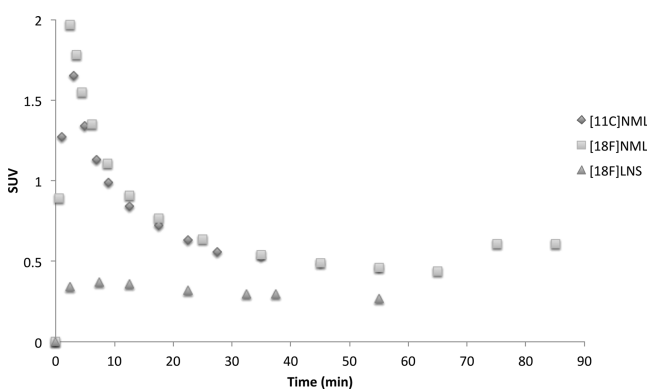


Figure 8. Nonhuman primate whole brain time-radioactivity curves for $[^{11}\text{C}]$ NML, $[^{18}\text{F}]$ NML, and $[^{18}\text{F}]$ LNS.

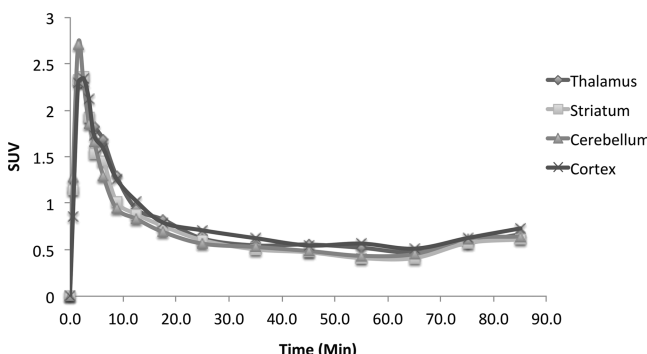
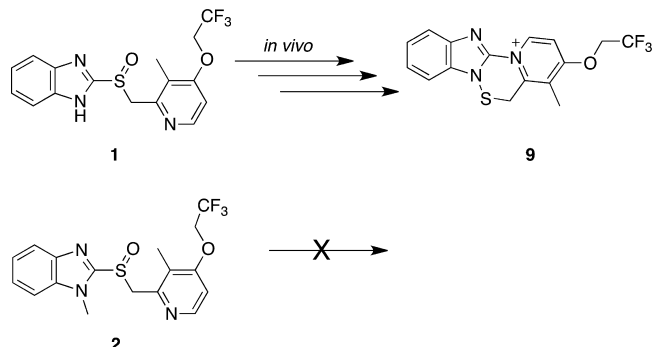


Figure 9. Regional time-radioactivity curves of the nonhuman primate brain for $[^{18}\text{F}]$ NML.

Similar results were expected when imaging nonhuman primates with $[^{18}\text{F}]$ lansoprazole. However, no brain uptake was observed for this radiotracer (Figure 7C and Figure 8). Additionally, while the known metabolites of lansoprazole are the sulfone and hydroxy derivatives,^{38,39,41} some apparent skull uptake of radioactivity suggests additional metabolic defluorination. Given the rodent imaging data, we assume that the lack of uptake in the brain is due to primate Pgp transporter involvement, but take a conservative view toward nonhuman primate safety and do not wish to block the Pgp to confirm the theory at this time. The mechanisms underlying Pgp transport are complex (for recent reviews see references^{42,43}), but the differences in primate brain permeability of the *N*-methyl lansoprazole derivatives and $[^{18}\text{F}]$ lansoprazole could possibly result from the additional methyl group on the benzimidazole ring of the former. The simplest explanation is that the methyl

group reduces affinity of the radiotracer for the Pgp efflux transporter, possibly by causing the methylated radiotracers to exist in a different rotamer to the parent lansoprazole. Alternatively, at lower pH values lansoprazole is known to undergo cyclization *in vivo* through a process involving the benzimidazole ring (Scheme 2).⁴⁴ This pathway could lead to a

Scheme 2. Anticipated Differences in Cyclization of Lansoprazole and *N*-Methyl Lansoprazole in Vivo



derivative of $[^{18}\text{F}]$ lansoprazole such as 9 that is a substrate for the Pgp transporter. However, the cyclization pathway is likely blocked when the benzimidazole is methylated, as in the case of 2 and 7, perhaps indicating that the Pgp substrate is not formed. Additional investigations that are beyond the scope of this paper are required to explore these theories further.

SUMMARY

The lansoprazole scaffold has been repurposed to prepare high-affinity radioligands with promise for quantification of aggregated tau levels in AD and PSP using PET imaging. The present work demonstrates that $[^{18}\text{F}]$ *N*-methyl lansoprazole, on account of the favorable half-life of fluorine-18 and its good brain entry in nonhuman primates, favorable kinetics, low white matter binding at imaging concentrations, high affinity for tau, and selectivity for tau over amyloid in both binding affinity experiments and autoradiography studies, is the lead compound for translation into human imaging trials.

EXPERIMENTAL SECTION

Chemistry. General Considerations. All the chemicals employed in the syntheses were sourced commercially, and used without further purification. Lansoprazole was purchased from Sigma-Aldrich. ^1H -nuclear magnetic resonance (NMR) spectra were obtained at 400 MHz on Varian NMR

spectrometer in CD₃OD solutions at room temperature with tetramethylsilane (TMS, $\delta = 0$) as an internal standard. ¹³C NMR spectra were obtained at 100 MHz and ¹⁹F-NMR spectra were obtained at 376 MHz. Chemical shifts (δ) are reported in ppm and coupling constants are reported in Hertz. Multiplicity is defined by s (singlet), d (doublet), t (triplet), q (quartet), and m (multiplet). High performance liquid chromatography (HPLC) was performed using a Shimadzu LC-2010A HT system equipped with a Bioscan B-FC-1000 radiation detector. Mass spectra were performed on a VG (Micromass) 70-250-S Magnetic sector mass spectrometer or Micromass AutoSpec Ultima Magnetic sector mass spectrometer employing the electrospray ionization (ESI) method.

2-((5-((2,2-Difluorovinyl)oxy)-3-methylpyridin-2-yl)methyl)sulfinyl)-1H-benzo[d]imidazole (3). In an oven-dried flask charged with a stir bar, lansoprazole 2 (0.30 g, 0.81 mmol) was dissolved in THF (3 mL) and cooled to -78 °C in a dry ice and acetone bath. To the reaction mixture a 1.6 M solution of *n*-butyl lithium in hexanes (1.52 mL, 2.44 mmol) was added dropwise. The reaction was stirred for 45 min at -78 °C; the reaction was quenched by the addition of a 1:1 mixture of THF and H₂O (1 mL). The mixture was warmed to room temperature and partitioned between ethyl acetate and H₂O. The aqueous layer was extracted with ethyl acetate (3×). The organic layers were combined, washed with brine, and dried over sodium sulfate. The organic layer was reduced in vacuo to prepare for purification. The product was purified by SiO₂ column chromatography (hexanes to ethyl acetate gradient column) to yield the title compound 3 as a white solid (0.063 g, 22%). R_f = 0.54 (EtOAc); ¹H NMR (400 MHz, MeOD-*d*₄) δ 8.19 (d, *J* = 5.7 Hz, 1H), 7.64 (br, 2H), 7.35 (br, 2H), 7.05 (d, *J* = 5.7 Hz, 1H), 6.61 (dd, *J*_{H-F} = 15 and 3.7 Hz, 1H), 4.83 (s, 2H), 2.23 (s, 3H); ¹³C NMR (100 MHz, DMSO-*d*₆) δ 161.46, 158.58, 156.27, 154.55, 151.85, 148.64, 123.43 (br), 122.52, 120.20, 112.83, 108.28, 105.19 (dd, *J*_{C-F} = 57 and 12 Hz), 60.33, 11.09; ¹⁹F NMR (376.3 MHz, MeOD-*d*₄) δ 98.42 (dd, *J*_{F-F} = 66 Hz, *J*_{H-F} = 15 Hz, 1F), 115.89 (dd, *J*_{F-F} = 66 Hz, *J*_{H-F} = 3.7 Hz, 1F); HR-MS (ESI) *m/z* calculated for C₁₆H₁₄F₂N₃O₂S, 350.0769; found, 350.0776 (M + H)⁺.

2-((4-((2,2-Difluorovinyl)oxy)-3-methylpyridin-2-yl)methyl)sulfinyl)-1-methyl-1H-benzo[d]imidazole (6). In an oven-dried flask charged with a stir bar, compound 3 (44.7 mg, 0.128 mmol) was dissolved in CH₂Cl₂ (1 mL). To the reaction mixture, DBU (23.37 mg, 0.153 mmol) and methyl iodide (36.6 mg, 0.256 mmol) were added and stirred at room temperature. After 1 h, the reaction was quenched with water (1 mL) and stirred for an additional 30 min. The product was extracted with CH₂Cl₂ (3x), and the organic layers were combined, washed with saturated sodium bicarbonate (aq.), and dried over sodium sulfate. The combined organic layers were reduced in *vacuo*, and the residue was purified by SiO₂ column chromatography (hexanes to ethyl acetate gradient column) to yield title compound 6 as a white solid (23.4 mg, 50%). R_f = 0.46 (EtOAc); ¹H NMR (400 MHz, MeOD-*d*₄) δ 8.15 (d, *J* = 5.7 Hz, 1H), 7.71 (d, *J* = 8.1 Hz, 1H), 7.61 (d, *J* = 8.2 Hz, 1H), 7.44 (t, *J* = 7.6 Hz, 1H), 7.36 (t, *J* = 8.1 Hz, 1H), 7.00 (d, *J* = 5.7 Hz, 1H), 6.61 (dd, *J*_{H-F} = 15 and 3.5 Hz, 1H), 5.03 (q, *J* = 13.7 Hz, 2H), 4.00 (s, 3H), 2.26 (s, 3H); ¹³C NMR (100 MHz, MeOD-*d*₄) δ 9.51, 29.68, 35.51, 58.27, 103.35, 103.49, 107.44, 110.29, 119.65, 122.75, 123.39, 124.71, 136.32, 141.51, 147.81, 151.64, 153.781; ¹⁹F NMR (376.3 MHz, MeOD-*d*₄) δ 98.40 (dd, *J*_{F-F} = 66 Hz, *J*_{H-F} = 15 Hz, 1F), 115.88 (dd, *J*_{F-F} = 66 Hz, *J*_{H-F} = 3.5 Hz, 1F); HR-MS (ESI) *m/z*

z calculated for C₁₇H₁₆F₂N₃O₂S, 364.0926; found, 364.0925 (M + H)⁺.

N-Methyl Lansoprazole ([¹²C]2). *N*-Methyl lansoprazole unlabeled reference standard was prepared as previously described and all spectral values were consistent with literature values.²⁴

Radiochemistry. General Considerations. Unless otherwise stated, reagents and solvents were commercially available and used without further purification: sodium chloride, 0.9% USP and sterile water for injection, USP were purchased from Hospira; ethanol was purchased from American Regent; HPLC grade acetonitrile was purchased from Fisher Scientific. Lansoprazole (used as both precursor for [¹¹C]*N*-methyl lansoprazole and unlabeled reference standard for [¹⁸F]-lansoprazole) was purchased from Sigma-Aldrich, and [¹²C]*N*-methyl lansoprazole (unlabeled reference standard for [¹¹C]*N*-methyl lansoprazole) was prepared as previously described.²⁴ Shimalite-nickel was purchased from Shimadzu; iodine was purchased from EMD; phosphorus pentoxide was purchased from Fluka; and molecular sieves were purchased from Alltech. Other synthesis components were obtained as follows: sterile filters were obtained from Millipore; sterile product vials were purchased from Hollister-Stier; C18-light Sep-Paks and Porapak-Q were purchased from Waters Corporation. Sep-Paks were flushed with 10 mL of ethanol followed by 10 mL of sterile water prior to use.

[¹¹C]Pittsburgh Compound B. [¹¹C]Pittsburgh Compound B was prepared as previously described.⁴⁵

[¹¹C]*N*-Methyl Lansoprazole ([¹¹C]2). [¹¹C]*N*-Methyl lansoprazole was prepared as previously described.²⁴

General Procedure for Drying [¹⁸F]Fluoride. Production of fluorine-18 labeled radiotracers was carried out using a TRACERLab FX_{FN} automated radiochemistry synthesis module (General Electric, GE). [¹⁸F]Fluoride was produced via the ¹⁸O(p,n)¹⁸F nuclear reaction using a GE PETTrace cyclotron (40 μ A beam for 15 min generated 33.3 GBq (900 mCi) of [¹⁸F]fluoride). The [¹⁸F]fluoride was delivered to the synthesis module (in a 1.5 mL bolus of [¹⁸O]water) and trapped on a QMA-light Sep-Pak to remove [¹⁸O]water. [¹⁸F]Fluoride was then eluted into the reaction vessel using aqueous potassium carbonate (3.5 mg in 0.5 mL of water). A solution of Kryptofix 2.2.2 (15 mg in 1 mL of acetonitrile) was then added to the reaction vessel and the [¹⁸F]fluoride was dried by evaporating the water-acetonitrile azeotrope. Evaporation was achieved by heating the reaction vessel to 80 °C and drawing full vacuum for 4 min. After this time, the reaction vessel was cooled to 60 °C and subjected to both an argon stream and vacuum draw simultaneously for another 4 min.

[¹⁸F]Lansoprazole (4). A solution of alkene precursor (3) (2–3 mg) in anhydrous DMSO (500 μ L) and isopropanol (36 μ L) was added to [¹⁸F]fluoride dried as described above, and the solution was heated at 90 °C with stirring for 3 min. The reaction mixture was cooled to 50 °C and diluted with semipreparative HPLC mobile phase (3 mL). The diluted reaction mixture was then purified by semipreparative HPLC (column: Phenomenex Luna PFP(2) 250 × 10 mm; mobile phase: 65% water in 35% acetonitrile (v/v); flow rate: 2.0 mL/min). The fraction corresponding to [¹⁸F]lansoprazole (typically eluting out between 27 and 32 min; see Figure S5 in Supporting Information for a typical semipreparative HPLC trace) was collected and transferred into a dilution flask containing sterile water (50 mL). The resulting solution was transferred through a Waters C18 1 cm³ Sep-Pak to collect the

desired product. The C18 Sep-Pak was then washed with sterile water (10 mL) to rinse residual acetonitrile to waste. [¹⁸F]Lansoprazole was eluted off into the product collection vial with ethanol for injection, USP (1.0 mL) and diluted with 0.9% sodium chloride for injection, USP (9.0 mL). The final isotonic formulation (10 mL) was passed through a 0.22 μ M Millex-GV sterile filter (Millipore, Billerica, MA) into a sterile vial to provide [¹⁸F]lansoprazole (typically 18–63 mCi, 2–7% nondecay-corrected radiochemical yield at end-of-synthesis based upon 900 mCi of [¹⁸F]fluoride, $n = 3$). The formulated dose of [¹⁸F]lansoprazole was found to have a pH of 5.0 and radiochemical purity was >95%.

[¹⁸F]N-Methyl Lansoprazole (**7**). The reaction vessel was cooled to 90 °C and alkene precursor **6** (3.5 mg) dissolved in DMSO (950 μ L) and aq. satd. ammonium chloride (5 μ L) was added to the reaction vessel. The reaction was stirred for 3 min at 90 °C, cooled to 50 °C, and quenched by the addition of HPLC solvent (3.5 mL, 30% acetonitrile). The diluted reaction mixture was then purified by semipreparative HPLC (column: Phenomenex Luna PFP(2) 250 \times 10 mm. Mobile phase: 65% water in 35% acetonitrile (v/v); flow rate, 2.0 mL/min). The fraction corresponding to [¹⁸F]N-methyl lansoprazole (typically eluting out at 44 min; see Figure S12 in Supporting Information for a typical semipreparative HPLC trace) was collected and transferred into a dilution flask containing sterile water (50 mL). The resulting solution was transferred through a Waters C18 1 cm³ Sep-Pak to collect the desired product. The sep-pak was subsequently rinsed with 10 mL of sterile water and eluted with dehydrated ethanol for injection (0.5 mL) into the collection vial containing saline (4.5 mL of 0.9% for injection, USP). Finally, the Sep-Pak was rinsed with an additional 5 mL of saline and the resulting isotonic formulated dose (10 mL) was transferred through a Millex-GV sterile filter (Millipore, Billerica, MA) into a sterile 10 mL dose vial to yield [¹⁸F]N-methyl lansoprazole (typically 27–60 mCi, 3–7% nondecay-corrected radiochemical yield at end-of-synthesis, based upon 900 mCi of [¹⁸F]fluoride, $n = 4$). The formulated dose of [¹⁸F]N-methyl lansoprazole was found to have a pH of 5.0 and radiochemical purity was >95%.

Semipreparative HPLC Column Maintenance. Following completion of a given radiosynthesis, careful maintenance of the Luna PFP(2) semipreparative HPLC column is recommended by Phenomenex to maximize column longevity. The column is conditioned between runs as follows. Flow rate, 3.0 mL/min; oven temperature, 40 °C. Run each of the following for 60 min each: 100% water, 100% THF, 100% MeCN, 65:35 MeCN:H₂O. The column is stored under 65:35 MeCN:H₂O.

Quality Control. Quality control of radiopharmaceutical doses was conducted using the following tests.

Visual Inspection. Doses were examined visually to confirm that they were clear, colorless, and free of particulate matter.

Dose pH. The pH of the doses was analyzed by applying a small amount of the dose to pH indicator strips and determined by visual comparison with the provided scale.

HPLC Analysis. radiochemical purity and dose concentration were determined using Shimadzu LC-2010A HT system equipped with a Bioscan B-FC-1000 radiation detector. [¹⁸F]Lansoprazole (**4**): column, Phenomenex Luna PFP(2) (150 \times 4.6 mm); mobile phase, 30% acetonitrile:70% H₂O; UV wavelength, 254 nm; flow rate, 2.0 mL/min; retention time, ~7.6 min. See Figure S6 in Supporting Information for a typical trace. [¹⁸F]N-Methyl lansoprazole (**4**): column, Phenomenex

Luna PFP(2) (150 \times 4.6 mm); mobile phase, 30% acetonitrile:70% H₂O; UV wavelength, 254 nm; flow rate, 2.0 mL/min; retention time, ~12.5 min. See Figure S12 in Supporting Information for a typical trace. HPLC analyses of [¹¹C]N-Methyl lansoprazole (**2**) and [¹¹C]Pittsburgh Compound B were conducted as previously described.^{24,45} For each compound, coinjection of the dose with unlabeled reference standard was performed to confirm compound identity, and radiochemical purity was ≥95%.

ASSOCIATED CONTENT

S Supporting Information

Spectra for all novel compounds synthesized, stability data and procedures for binding affinity experiments, microPET imaging, autoradiography, and immunohistochemistry. This material is available free of charge via the Internet at <http://pubs.acs.org>.

AUTHOR INFORMATION

Corresponding Author

*P. J. H. Scott. E-mail: pjhscott@umich.edu. Tel.: +1 (734) 615-1756. Fax: +1 (734) 615-2557.

Author Contributions

[†]The manuscript was written through contributions of all authors. All authors have given approval to the final version of the manuscript. These authors contributed equally.

Funding

Financial support of this work from the National Institute of Biomedical Imaging and Bioengineering, part of the National Institutes of Health (under Award Number T32-EB005172) is gratefully acknowledged. The content of this article is solely the responsibility of the authors and does not necessarily represent the official views of the National Institutes of Health. Additional funding for this research from the Alzheimer's Association (under award number NIRP-14-305669), the University of Michigan Office of the Vice President for Research, and the University of Michigan Undergraduate Research Opportunity Program (UROP) is gratefully acknowledged. The Michigan Alzheimer's Disease Center is funded by the National Institute of Aging (under Award Number P50-AG08671) as well as a gift from an anonymous donor.

Notes

The authors declare no competing financial interest.

ACKNOWLEDGMENTS

The authors thank the Michigan Alzheimer's Disease Center Brain Bank for selecting and providing brain samples.

ABBREVIATIONS

AD, Alzheimer's disease; HITF, heparin-induced tau filaments; IPA, isopropanol; K-2.2.2, Kryptofix 2.2.2; LNS, lansoprazole; MAP, maximum a posteriori; NML, N-methyl lansoprazole; Pgp, P-glycoprotein transporter; PFP, perfluorophenyl; PiB, Pittsburgh Compound B; QMA, quarternary methylammonium; RCY, radiochemical yield; ROI, region of interest; SA, specific activity; TACs, time-radioactivity curves

REFERENCES

- (1) Thies, W., and Bleiler, L. (2012) 2012 Alzheimer's disease facts and figures. *Alzheimer's Dementia* 8, 131–168.
- (2) Knopman, D. S., DeKosky, S. T., Cummings, J. L., Chui, H., Corey-Bloom, J., Relkin, N., Small, G. W., Miller, B., and Stevens, J. C.

- (2001) Practice parameter: diagnosis of dementia (an evidence-based review). *Neurology* 56, 1143–1153.
- (3) Rinne, J. O., Brooks, D. J., Rossor, M. N., Fox, N. C., Bullock, R., Klunk, W. E., Mathis, C. A., Blennow, K., Barakos, J., Okello, A. A., Rodriguez Martinez de Llano, S., Liu, E., Koller, M., Gregg, K. M., Schenk, D., Black, R., and Grundman, M. (2010) ^{11}C -PiB PET assessment of change in fibrillar amyloid- β load in patients with Alzheimer's disease treated with bapineuzumab: a phase 2, double-blind, placebo-controlled, ascending-dose study. *Lancet Neurol.* 9, 363–372.
- (4) Klunk, W. E., Engler, H., Nordberg, A., Wang, Y., Blomqvist, G., Holt, D. P., Bergström, M., Savitcheva, I., Huang, G. F., Estrada, S., Ausén, B., Debnath, M. L., Barletta, J., Price, J. C., Sandell, J., Lopresti, B. J., Wall, A., Koivisto, P., Antoni, G., Mathis, C. A., and Långstrom, B. (2004) Imaging brain amyloid in Alzheimer's disease with Pittsburgh compound-B. *Ann. Neurol.* 55, 306–319.
- (5) Johnson, K. A., Sperling, R. A., Gidicin, C. M., Carmasin, J. S., Maye, J. E., Coleman, R. E., Reiman, E. M., Sabbagh, M. N., Sadowsky, C. H., Fleisher, A. S., Murali-Doraismamy, P., Carpenter, A. P., Clark, C. M., Joshi, A. D., Lu, M., Grundman, M., Mintun, M. A., Pontecorvo, M. J., and Skovronsky, D. M. (2013) Florbetapir (F18-AV-45) PET to assess amyloid burden in Alzheimer's disease dementia, mild cognitive impairment, and normal aging. *Alzheimer's Dementia* 9 (Suppl.), S72–S83.
- (6) Hatashita, S., Yamasaki, H., Suzuki, Y., Tanaka, K., Wakebe, D., and Hayakawa, H. (2013) $[^{18}\text{F}]$ Flutemetamol amyloid-beta PET imaging compared with $[^{11}\text{C}]$ PIB across the spectrum of Alzheimer's disease. *Eur. J. Nucl. Med. Mol. Imaging*, DOI: 10.1007/s00259-00013-02564-y.
- (7) Barthel, H., and Sabri, O. (2011) Florbetaben to trace amyloid- β in the Alzheimer brain by means of PET. *J. Alzheimer's Dis.* 26 (Suppl. 3), 117–121.
- (8) Giannakopoulos, P., Herrmann, F. R., Bussière, T., Bouras, C., Kövari, E., Perl, D. P., Morrison, J. H., Gold, G., and Hof, P. R. (2003) Tangle and neuron numbers, but not amyloid load, predict cognitive status in Alzheimer's disease. *Neurology* 60, 1495–1500.
- (9) Ludolph, A. C., Kassubek, J., Landwehrmeyer, B. G., Mandelkow, E., Mandelkow, E.-M., Burn, D. J., Caparros-Lefebvre, D., Frey, K. A., de Yebenes, J. G., Gasser, T., Heutink, P., Höglunger, G., Jamrozik, Z., Jellinger, K. A., Kazantsev, A., Kretzschmar, H., Lang, A. E., Litvan, I., Lucas, J. J., McGeer, P. L., Melquist, S., Oertel, W., Otto, M., Paviour, D., Reum, T., Saint-Raymond, A., Steele, J. C., Tolnay, M., Tumani, H., van Swieten, J. C., Vanier, M. T., Vonsattel, J.-P., Wagner, S., and Wszolek, Z. K. (2009) Tauopathies with parkinsonism: clinical spectrum, neuropathologic basis, biological markers, and treatment options. *Eur. J. Neurol.* 16, 297–309.
- (10) Ono, M., Hayashi, S., Matsumura, K., Kimura, H., Okamoto, Y., Ihara, M., Takahashi, R., Mori, H., and Saji, H. (2011) Rhodanine and thiohydantoin derivatives for detecting tau pathology in Alzheimer's brains. *ACS Chem. Neurosci.* 2, 269–275.
- (11) Okamura, N., Suemoto, T., Furumoto, S., Suzuki, M., Shimadzu, H., Akatsu, H., Yamamoto, T., Fujiwara, H., Nemoto, M., Maruyama, M., Arai, H., Yanai, K., Sawada, T., and Kudo, Y. (2005) Quinoline and ben-zimidazole derivatives: candidate probes for in vivo imaging of tau pathology in Alzheimer's disease. *J. Neurosci.* 25, 10857–10862.
- (12) Fodero-Tavoletti, M. T., Okamura, N., Furumoto, S., Mulligan, R. S., Connor, A. R., McLean, C. A., Cao, D., Rigopoulos, A., Cartwright, G. A., O'Keefe, G., Gong, S., Adlard, P. A., Barnham, K. J., Rowe, C. C., Masters, C. L., Kudo, Y., Cappai, R., Yanai, K., and Villemagne, V. L. (2011) ^{18}F -THK523: a novel in vivo tau imaging ligand for Alzheimer's disease. *Brain* 134, 1089–1100.
- (13) Okamura, N., Furumoto, S., Harada, R., Tago, T., Yoshikawa, T., Fodero-Tavoletti, M. T., Mulligan, R. S., Villemagne, V. L., Akatsu, H., Yamamoto, T., Arai, H., Iwata, R., Yanai, K., and Kudo, Y. (2013) Novel ^{18}F -labeled arylquinoline derivatives for noninvasive imaging of tau pathology in Alzheimer disease. *J. Nucl. Med.* 54, 1420–1427.
- (14) Harada, R., Okamura, N., Furumoto, S., Tago, T., Maruyama, M., Higuchi, M., Yoshikawa, T., Arai, H., Iwata, R., Kudo, Y., and Yanai, K. (2013) Comparison of the binding characteristics of [18F]THK-523 and other amyloid imaging tracers to Alzheimer's disease pathology. *Eur. J. Nucl. Med. Mol. Imaging* 40, 125–132.
- (15) Xia, C. F., Arteaga, J., Chen, G., Gangadharmath, U., Gomez, L. F., Kasi, D., Lam, C., Liang, Q., Liu, C., Mochalra, V. P., Mu, F., Sinha, A., Su, H., Szardenings, A. K., Walsh, J. C., Wang, E., Yu, C., Zhang, W., Zhao, T., and Kolb, H. C. (2013) $[^{18}\text{F}]$ T807, a novel tau positron emission tomography imaging agent for Alzheimer's disease. *Alzheimer's Dementia* 9, 666–676.
- (16) Chien, D. T., Bahri, S., Szardenings, A. K., Walsh, J. C., Mu, F., Su, M. Y., Shankle, W. R., Elizarov, A., and Kolb, H. C. (2013) Early clinical PET imaging results with the novel PHF-tau radioligand [F-18]-T807. *J. Alzheimer's Dis.* 34, 457–468.
- (17) Chien, D. T., Szardenings, A. K., Bahri, S., Walsh, J. C., Mu, F., Xia, C., Shankle, W. R., Lerner, A. J., Su, M. Y., Elizarov, A., and Kolb, H. C. (2014) Early Clinical PET Imaging Results with the Novel PHF-Tau Radioligand [F18]-T808. *J. Alzheimer's Dis.* 38, 171–184.
- (18) Zhang, W., Arteaga, J., Cashion, D. K., Chen, G., Gangadharmath, U., Gomez, L. F., Kasi, D., Lam, C., Liang, Q., Liu, C., Mochalra, V. P., Mu, F., Sinha, A., Szardenings, A. K., Wang, E., Walsh, J. C., Xia, C., Yu, C., Zhao, T., and Kolb, H. C. (2012) A highly selective and specific PET tracer for imaging of tau pathologies. *J. Alzheimer's Dis.* 31, 601–612.
- (19) Maruyama, M., Shimada, H., Suhara, T., Shinotoh, H., Ji, B., Maeda, J., Zhang, M. R., Trojanowski, J. Q., Lee, V. M., Ono, M., Masamoto, K., Takano, H., Sahara, N., Iwata, N., Okamura, N., Furumoto, S., Kudo, Y., Chang, Q., Saido, T. C., Takashima, A., Lewis, J., Jang, M. K., Aoki, I., Ito, H., and Higuchi, M. (2013) Imaging of tau pathology in a tauopathy mouse model and in Alzheimer patients compared to normal controls. *Neuron* 79, 1094–1108.
- (20) Small, G. W., Kepe, V., Ercoli, L. M., Siddarth, P., Bookheimer, S. Y., Miller, K. J., Lavretsky, H., Burggren, A. C., Cole, G. M., Vinters, H. V., Thompson, P. M., Huang, S. C., Satyamurthy, N., Phelps, M. E., and Barrio, J. R. (2006) PET of brain amyloid and tau in mild cognitive impairment. *N. Engl. J. Med.* 355, 2652–2663.
- (21) Kepe, V., Bordelon, Y., Boxer, A., Huang, S. C., Liu, J., Thiede, F. C., Mazziotta, J. C., Mendez, M. F., Donoghue, N., Small, G. W., and Barrio, J. R. (2013) PET imaging of neuropathology in tauopathies: progressive supranuclear palsy. *J. Alzheimer's Dis.* 36, 145–153.
- (22) Rojo, L. E., Alzate-Morales, J., Saavedra, I. N., Davies, P., and Maccioni, R. B. (2010) Selective interaction of lansoprazole and astemizole with tau polymers: potential new clinical use in diagnosis of Alzheimer's disease. *J. Alzheimer's Dis.* 19, 573–589.
- (23) Riss, P. J., Brichard, L., Ferrari, V., Williamson, D. J., Fryer, T. D., Hong, Y. T., Baron, J.-C., and Aigbirhio, F. I. (2013) Radiosynthesis and characterization of astemizole derivatives as lead compounds toward PET imaging of τ -pathology. *Med. Chem. Comm.* 4, 852–855.
- (24) Shao, X., Carpenter, G. M., Desmond, T. J., Sherman, P., Quesada, C. A., Fawaz, M., Brooks, A. F., Kilbourn, M. R., Albin, R. L., Frey, K. A., and Scott, P. J. H. (2012) Evaluation of $[^{11}\text{C}]$ N-methyl lansoprazole as a radiopharmaceutical for PET imaging of tau neurofibrillary tangles. *ACS Med. Chem. Lett.* 3, 936–941.
- (25) Villemagne, V. L., Furumoto, S., Fodero-Tavoletti, M. T., Harada, R., Mulligan, R. S., Kudo, Y., Masters, C. L., Yanai, K., Rowe, C. C., and Okamura, N. (2012) The challenges of tau imaging. *Future Neurol.* 7, 409–421.
- (26) Small, G. W., Agdeppa, E. D., Kepe, V., Satyamurthy, N., Huang, S. C., and Barrio, J. R. (2002) In vivo brain imaging of tangle burden in humans. *J. Mol. Neurosci.* 19, 323–327.
- (27) Jensen, J. R., Cisek, K., Funk, K. E., Naphade, S., Schafer, K. N., and Kuret, J. (2011) Research towards tau imaging. *J. Alzheimer's Dis.* 26 (Suppl. 1), 147–157.
- (28) Maccioni, R. B., Rojo, L. E., Kuljis, A. R. (2010) Benzimidazole-derived compounds used as markers in the case of neurodegenerative diseases. WO Patent WO2010013127 A1.
- (29) Riss, P. J., Ferrari, V., Brichard, L., Burke, P., Smith, R., and Aigbirhio, F. I. (2012) Direct, nucleophilic radiosynthesis of

- [¹⁸F]trifluoroalkyl tosylates: improved labelling procedures. *Org. Biomol. Chem.* 10, 6980–6986.
- (30) Riss, P. J., and Aigbirhio, F. I. (2011) A simple, rapid procedure for nucleophilic radiosynthesis of aliphatic [¹⁸F]trifluoromethyl groups. *Chem. Commun.* 47, 11873–11875.
- (31) Aigbirhio, F. I., Pike, V. W., Waters, S. L., Makepeace, J., and Tanner, R. J. N. (1993) Efficient and selective labelling of the CFC alternative, 1,1,1,2-tetrafluoroethane, with ¹⁸F in the 1-Position. *J. Chem. Soc., Chem. Commun.*, 1064–1065.
- (32) Eckelman, W. C., Kilbourn, M. R., and Mathis, C. A. (2006) Discussion of targeting proteins *in vivo*: *in vitro* guidelines. *Nucl. Med. Biol.* 33, 449–451.
- (33) Schafer, K. N., Kim, S., Matzavinos, A., and Kuret, J. (2012) Selectivity requirements for diagnostic imaging of neurofibrillary lesions in Alzheimer's disease: a simulation study. *Neuroimage* 60, 1724–1733.
- (34) Delhotal Landes, B., P, P. J., and B, F. (1995) Clinical pharmacokinetics of lansoprazole. *Clin. Pharmacokinet.* 28, 458–470.
- (35) Zhang, D., Zhang, Y., Liu, M., Wang, X., Yang, M., Han, J., and Liu, H. (2013) Pharmacokinetics of lansoprazole and its main metabolites after single and multiple intravenous doses in healthy Chinese subjects. *Eur. J. Drug Metab. Pharmacokinet.* 38, 209–215.
- (36) Gremse, D. A. (2001) Lansoprazole: pharmacokinetics, pharmacodynamics and clinical uses. *Expert Opin. Pharmacother.* 2, 1663–1670.
- (37) Karol, M. D., Machinist, J. M., and Cavanaugh, J. M. (1997) Lansoprazole pharmacokinetics in subjects with various degrees of kidney function. *Clin. Pharmacol. Ther.* 61, 450–458.
- (38) Kim, K.-A., Kim, M.-J., Park, J.-Y., Shon, J.-H., Yoon, Y.-R., Lee, S.-S., Liu, K.-H., Chun, J.-H., Hyun, M.-H., and Shin, J.-G. (2003) Stereoselective metabolism of lansoprazole by human liver cytochrome P450 enzymes. *Drug Metab. Dispos.* 31, 1227–1234.
- (39) Pearce, R. E., Rodrigues, A. D., Goldstein, J. A., and Parkinson, A. (1996) Identification of the human P450 enzymes involved in lansoprazole metabolism. *J. Pharmacol. Exp. Ther.* 277, 805–816.
- (40) Uchida, Y., Ohtsuki, S., Katsukura, Y., Ikeda, C., Suzuki, T., LKamiie, J., and Terasaki, T. (2011) Quantitative targeted absolute proteomics of human blood-brain barrier transporters and receptors. *J. Neurochem.* 117, 333–345.
- (41) Pichard, L., Curi-Pedrosa, R., Bonfils, C., Jacqz-Aigrain, J., Domergue, J., Joyeux, H., Cosme, J., Guengerich, F. P., and Maurel, P. (1995) Oxidative metabolism of lansoprazole by human liver cytochromes P450. *Mol. Pharmacol.* 47, 410–418.
- (42) Sharom, F. J. (1997) The P-glycoprotein efflux pump: how does it transport drugs? *J. Membr. Biol.* 160, 161–175.
- (43) Sauna, Z. E., Smith, M. M., Müller, M., Kerr, K. M., and Ambudkar, S. V. (2001) The mechanism of action of multidrug-resistance-linked P-glycoprotein. *J. Bioenerg. Biomembr.* 33, 481–491.
- (44) Shin, J. M., Cho, Y. M., and Sachs, G. (2004) Chemistry of covalent inhibition of the gastric (H⁺, K⁺)-ATPase by proton pump inhibitors. *J. Am. Chem. Soc.* 126, 7800–7811.
- (45) Shao, X., Hoareau, R., Runkle, A. C., Tluczek, L. J. M., Hockley, B., Henderson, B. D., and Scott, P. J. H. (2011) Highlighting the versatility of the Tracerlab synthesis modules. Part 2: fully automated production of [¹¹C]-labeled radiopharmaceuticals using a Tracerlab FXC-Pro. *J. Labelled Compd. Radiopharm.* 54, 819–838.